Modeling of Transient Turing-Type Patterns in the Closed Chlorine Dioxide-Iodine-Malonic Acid-Starch Reaction System

Sándor Kádár, István Lengyel, and Irving R. Epstein*

Department of Chemistry and Center for Complex Systems, Brandeis University, Waltham, Massachusetts 02254-9110

Received: July 28, 1994; In Final Form: October 24, 1994[⊗]

The time development of the chlorine dioxide-iodine-malonic acid-starch reaction, which shows transient Turing patterns, traveling waves, and oscillations in an inhomogeneous closed system, is simulated with a six-variable model in one and two spatial dimensions. The results of numerical simulations are compared with experiments, and the agreement is found to be excellent.

Introduction

Since the discovery of experimental chemical examples of symmetry-breaking Turing patterns in 1990,[1] several groups have attempted to model these fascinating patterns using a variety of models. The computational challenge of simulating reaction-diffusion systems makes the use of strongly simplified models attractive, since with such schemes it may be feasible to make analytical predictions, and it is relatively easy to carry out numerical simulations. There are two approaches: one is to use an abstract model that is chemically unrelated to the experimental system in order to make qualitative predictions; the other is to employ a simplified model derived from the real dynamics of the system. The most popular abstract models are the Schnackenberg[2] and Brusselator[3] schemes, because these have already been analyzed in great detail, are numerically stable, and do not require stiff solvers to evaluate the partial differential equation systems. Although these models show some similarities to the experimental systems in their bifurcation sequences and qualitative patterns,[4-6] they do not permit quantitative comparision or prediction of new features at specific parameter values of the real chemical system. The alternative path, which we have followed earlier, is to simplify a chemically reasonable model to two variables[7] and to make predictions based on analysis of the simplified reaction-diffusion system. We have shown that a simplified model of the chlorine dioxide-iodine-malonic acid (CDIMA) system accurately predicts the wavelength of Turing structures,[8,9] the position of the structures in an imposed gradient,[10] the appearance of transient Turing patterns in a batch system[11] and the interaction of Turing and Hopf bifurcations.[12] Moreover, recent numerical studies suggest that there may be qualitative differences regarding the subcriticality of the Turing bifurcation between the above abstract models and our chemically derived, two-variable model.[13] In our simplified model, however, parameters related to the reactants present in great excess must be kept constant. Consequently, the full time development of the Turing patterns, particularly their transition to waves, cannot be modeled.

Here we present numerical simulations with a six-variable model based on four component stoichiometric processes. This model has already been found to give good agreement with the experimentally determined homogeneous behavior of the system.[7] We have tested two different numerical methods and have compared the results of our simulations in one and two spatial dimensions with experiment.

The Model

The primary purpose of this work is to model and characterize the time development of the CDIMA reaction in a closed system, how and when Turing-type patterns arise and vanish as the system moves along its reaction coordinate from a far-from-equilibrium, inhomogeneous, initial state to a final, homogeneous, chemical equilibrium. Figure 1 shows typical transient Turing type patterns found in a closed system .[11] The patterns are interacting hexagons, as confirmed by Fourier analysis.[11] To describe the time development of the homogeneous system we require three component processes. We have also shown that starch, which is used as a color indicator, has a specific chemical effect, binding iodine and iodide in an unreactive, immobile complex,[8,14] This complexation reaction decreases the effective diffusivity of the activator (in Turing's sense), iodide, making possible the emergence of Turing patterns. If the complexation equilibrium is rapid, the incorporation of this effect into our two-variable model can be accomplished without increasing the number of variables.[14] The binding of iodine and iodide by starch is a complex reaction:[15] it has variable stoichiometry depending on the iodide concentration and on the mean degree of polymerization of the amylose. Also, there is a high degree of cooperativity for iodine binding in the complex.[16,17] Under the experimental conditions, this complex equilibrium system may be simplified because of the high excess of iodine to iodide. In this case we can represent the process by a single equlibrium step. The chemistry of the CDIMA-starch chemical system can be described by the following reactions:

$$\mathrm{MA} + \mathrm{I_2} \rightarrow \mathrm{IMA} + \mathrm{I^-} + \mathrm{H^+}$$

$$r_1 = k_{1a}[\mathrm{MA}][\mathrm{I_2}]/(k_{1b} + [\mathrm{I_2}])$$

$$\mathrm{ClO_2} + \mathrm{I^-} \rightarrow \mathrm{ClO_2^-} + {}^1/_2\mathrm{I_2}$$

$$r_2 = k_2[\mathrm{ClO_2}][\mathrm{I^-}]$$

$$\mathrm{ClO_2^-} + 4\mathrm{I^-} + 4\mathrm{H^+} \rightarrow 2\mathrm{I_2} + \mathrm{Cl^-} + 2\mathrm{H_2O}$$

$$r_3 = k_{3a}[\mathrm{ClO_2^-}][\mathrm{I^-}][\mathrm{H^+}] + k_{3b}[\mathrm{ClO_2^-}][\mathrm{I_2}][\mathrm{I^-}]/(u + [\mathrm{I^-}]^2)$$

$$\mathrm{S} + \mathrm{I^-} + \mathrm{I_2} \rightleftharpoons \mathrm{SI_3^-}$$

$$r_4 = k_4[\mathrm{S}][\mathrm{I_2}][\mathrm{I^-}] - k_{-4}[\mathrm{SI_3^-}] \qquad (1)$$

where [S] represents the concentration of starch per six monomer

[⊗] Abstract published in *Advance ACS Abstracts,* March 1, 1995.

0022-3654/95/2099-4054$09.00/0

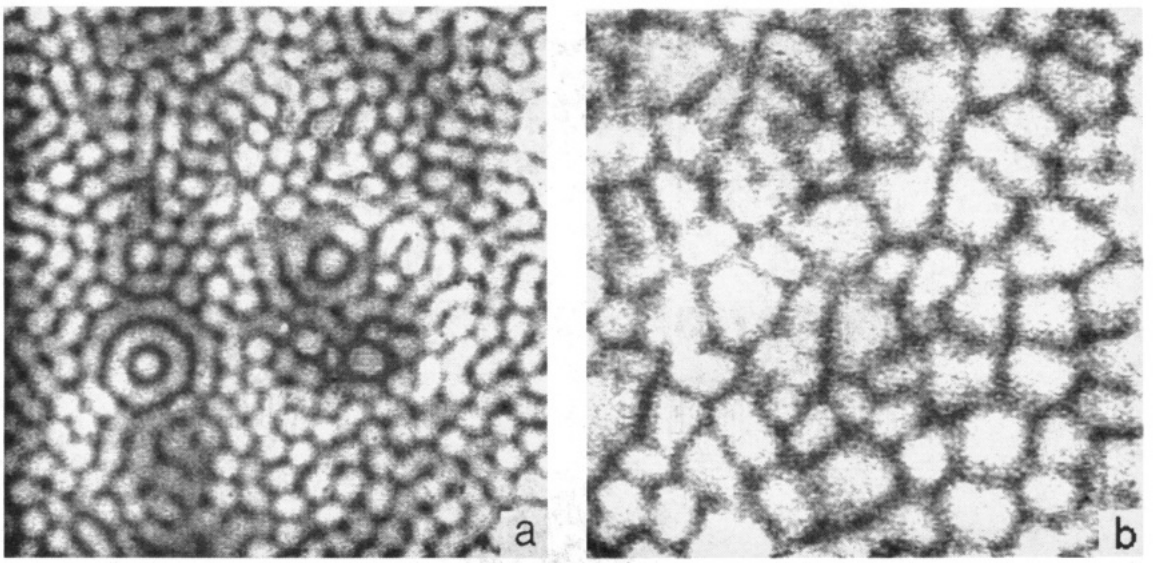

Figure 1. Basic types of Turing structures found experimentally in closed system: (a) interacting hexagons; (b) network-like structures ($[ClO_2]_0 = 6 \times 10^{-3}$ M, $[I_2]_0 = 8.2 \times 10^{-3}$ M, $[H^+] = 10^{-2}$ M, $[MA]_0 = 4 \times 10^{-3}$ M (a) and $[MA]_0 = 2 \times 10^{-3}$ M (b)).

units needed to form a complete helix. If the concentration of iodide were not much smaller than that of iodine, assuming the above stoichiometry for the last reaction would modify the free iodine concentration significantly compared to the real situation. The partial differential equation system for reactions 1 is

$$\partial[MA]/\partial t = -r_1 + D_{MA}\nabla^2[MA]$$

$$\partial[I_2]/\partial t = -r_1 + {}^1/_2 r_2 + 2r_3 - r_4 + D_{I_2}\nabla^2[I_2]$$

$$\partial[ClO_2]/\partial t = -r_2 + D_{ClO_2}\nabla^2[ClO_2]$$

$$\partial[I^-]/\partial t = -r_1 - r_2 - 4r_3 - r_4 + D_{I^-}\nabla^2[I^-]$$

$$\partial[ClO_2^-]/\partial t = r_2 - r_3 + D_{ClO_2^-}\nabla^2[ClO_2^-]$$

$$\partial[SI_3^-]/\partial t = r_4 + D_{SI_3^-}\nabla^2[SI_3^-] \qquad (2)$$

The parameters and diffusion coefficients are listed in Table 1. Note that the diffusivities of the starch and of the starch–triiodide complex are considered to be zero because of the large molecular weight and high concentration of the starch. Under these conditions the starch molecules become interlocked, effectively preventing their diffusion. The structure of the solution resembles that of a dilute gel. The diffusion terms on the right-hand side of eqs 2 were approximated by finite differences in both one and two spatial dimensions. Although the experiments were run with zero flux boundary conditions, we used periodic boundary conditions in the simulations to decrease the effects of the boundaries. In the real experimental system the size of the dish in which the reaction was carried out was at least 200 times larger than the wavelength of the patterns. Computational limitations prevent our conducting simulations with sufficiently high spatial resolution for such a large system. With periodic boundary conditions, the structures have the same characteristics throughout the system.

To solve the partial differential equation system (2), we used two stiff differential equation solvers. The first was a semi-implicit Runge–Kutta (SRK) method[18] with a banded linear equation system solver. The other was the VODPK program package developed by Hindmarsh et al. in the family of reduced storage matrix solvers.[19–23] VODPK uses the Krylov subspace method: it has significantly decreased memory requirements

TABLE 1: Parameters of the Model of the CDIMA–Starch Reaction System

rate or diffusion constant	value at 25 °C	EA (kJ mol^{-1})	value at 4 °C	ref
k_{1a} (s^{-1})	7.5×10^{-3}	81.5	6.2×10^{-4}	8
k_{1b} (M)	5×10^{-5}		5×10^{-5}	8
k_2 (M^{-1} s^{-1})	6×10^3	62.0	9.0×10^2	8
k_{3a} (M^{-2} s^{-1})	460	51.4	100	24
k_{3b} (s^{-1})	2.65×10^{-3}	110.0	9.2×10^{-5}	24
α (M^2)	1×10^{-14}		1×10^{-14}	7
k_4 (M^{-2} s^{-1})[a]			6×10^5	our estimation
k_{-4} (s^{-1})[a]			1.0	our estimation
$10^5 D_{ClO_2^-}$[b]	1.5		0.75	estimated from mobility data
$10^5 D_{I^-}$	1.4		0.7	25
$10^5 D_{ClO_2}$	1.5		0.75	as ClO_2^-
$10^5 D_{I_2}$	1.2		0.6	estimated values for I^- and I_3^- 25
$10^5 D_{MA}$	0.8		0.4	estimated from mobility data
D_{starch}	0($<10^{-7}$)		0($<10^{-7}$)	our estimation

[a] These rate constants were set to values in the calculations with the six-variable model that ensure that they are not rate-limiting steps. These values are smaller than anticipated from temperature jump relaxation data. Choosing higher values will not modify any of the results. [b] All diffusion coefficients in cm^2 s^{-1}.

compared to other GEAR-related routines. In the one spatial dimensional simulations the average CPU time on an IBM RISC Model 360 workstation was about 10 times shorter using VODPK without preconditioning (3 min) than using SRK. The actual CPU time strongly depended on the time development of the reaction; if homogeneous oscillations with short period appeared, significantly longer CPU times were required. Both methods gave the same results in the simulations. Because of its greater effectiveness, VODPK was used for all the simulations in two spatial dimensions. In these calculations the memory requirement was about 26 megabytes with 160×160 grid points and 6 variables.

Results

In the experimental system Turing patterns arise only in a narrow range of concentrations. For the simulations we kept all concentrations constant except that of malonic acid ([MA]), which was varied between 2×10^{-3} and 7×10^{-3} M. As [MA] increases, the wavelength of the patterns increases, they develop

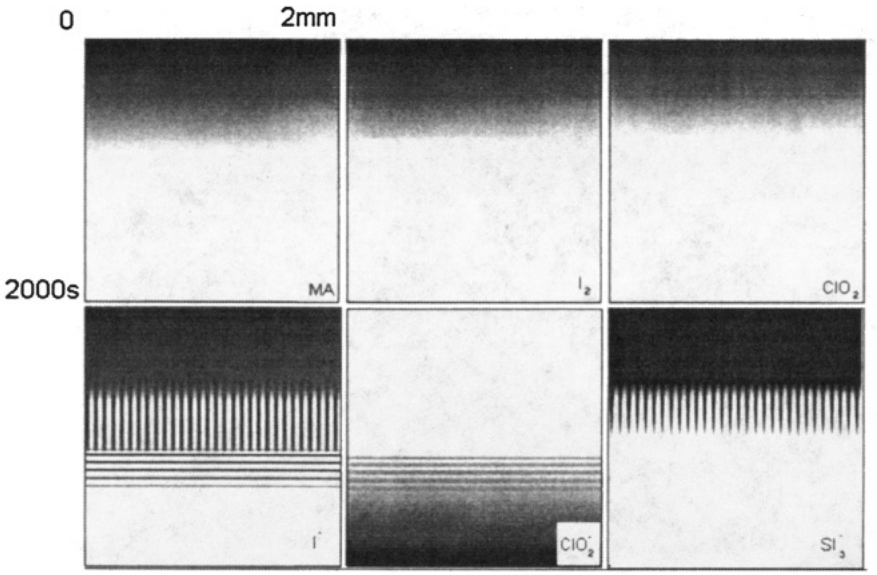

Figure 2. Time development of concentrations in one-dimensional simulation ($[ClO_2]_0 = 6 \times 10^{-3}$ M, $[I_2]_0 = 8.2 \times 10^{-3}$ M, $[H^+] = 10^{-2}$ M, $[MA]_0 = 3 \times 10^{-3}$ M).

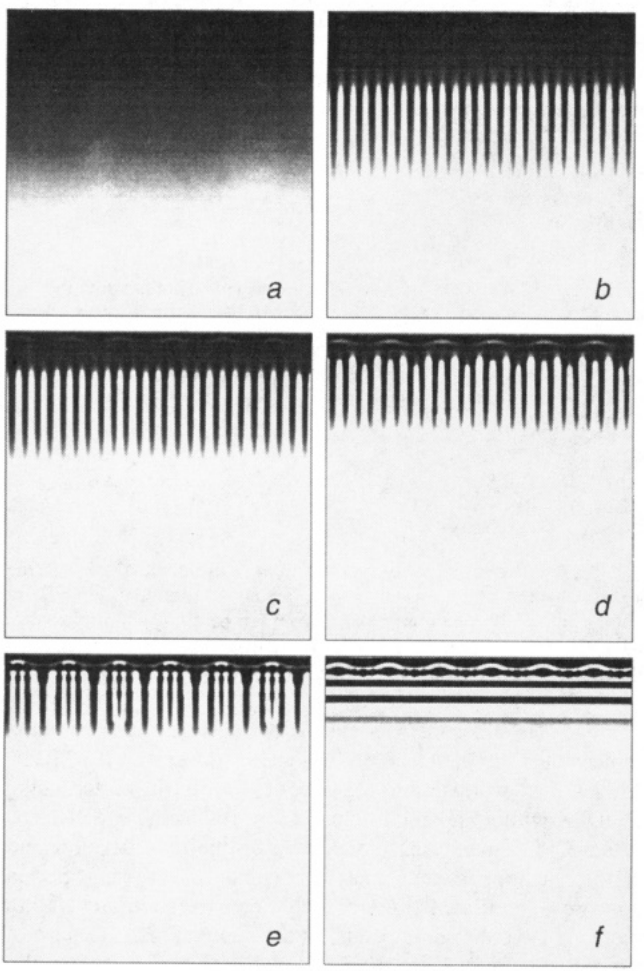

Figure 3. Dependence of simulated time development on $[MA]_0$ in one spatial dimension ($[ClO_2]_0 = 6 \times 10^{-3}$ M, $[I_2]_0 = 8.2 \times 10^{-3}$ M, $[H^+] = 10^{-2}$ M, $[MA]_0 = 2 \times 10^{-3}$ (a), $[MA]_0 = 2.5 \times 10^{-3}$ (b), $[MA]_0 = 3 \times 10^{-3}$ (c), $[MA]_0 = 4 \times 10^{-3}$ (d), $[MA]_0 = 5 \times 10^{-3}$ (e), $[MA]_0 = 7 \times 10^{-3}$ (f), horizontally, spatial coordinate 5 mm; vertically, time 2000 s).

more quickly, and they live for a shorter time before disappearing. The patterns generally seen are interacting hexagons or stripes, whose position does not change in time. The patterns eventually give way to either traveling waves or homogeneous bulk oscillations. The structures require a few hundred seconds to develop; they then remain stationary for 10−30 min, depending on the malonic acid concentration. In the experiments the thickness of the solution layer was comparable with the Turing wavelength, thereby preventing the formation of three-dimensional structures. Consequently the structures can be considered as two dimensional. Since the experiments were run at 4 °C, parameters at this temperature were used in the calculations.

One-dimensional simulations are useful for rapid calculation of the time development of the reaction and for estimating the wavelength. In Figure 2 we show the time development of all six variables in one spatial dimension. Each variable is scaled independently, since the maximum concentrations of the components are very different. On the eight-bit gray scale 0 (black) represents the highest and 255 (white) the lowest concentration of each species. While the concentrations of the reactants ClO_2, I_2 and MA decrease monotonically, the intermediates I^-, ClO_2^-, and SI_3^- have patterned distributions both in space and in time. After about 8 min of reaction time, transient Turing-type patterns appear. Their position does not change in time; their fading away can be seen in the time development of $[SI_3^-]$, which is the visually observable species. The wavelength is 0.17 mm, comparable to the experimental wavelength of about 0.2 mm. After the disappearance of Turing patterns, homogeneous oscillations appear. This transition is best seen in the $[I^-]$ and $[ClO_2^-]$ frames. The simulations contain 400 grid points across the 5 mm distance, which gives 80 grid points/mm resolution. The wavelength and time development of the patterns were independent of the resolution so long as it is higher than 60 points/mm.

The calculations were started from slightly inhomogeneous initial concentrations. The concentration of chlorine dioxide was perturbed with a sinusoidal function whose amplitude was 1−2% of the total $[ClO_2]$. The wavelength and time development of the structures were independent of the wavelength of the sinusoidal function, but structures arose only if the perturbation amplitude exceeded 0.1% of $[ClO_2]$. Perturbations with different wavelengths and amplitudes led to the same structures as long as the amplitude was less than 5%. In the real experimental system, inhomogeneous perturbations are always present, because contaminants in the starch lead to small local variations in $[ClO_2]$.

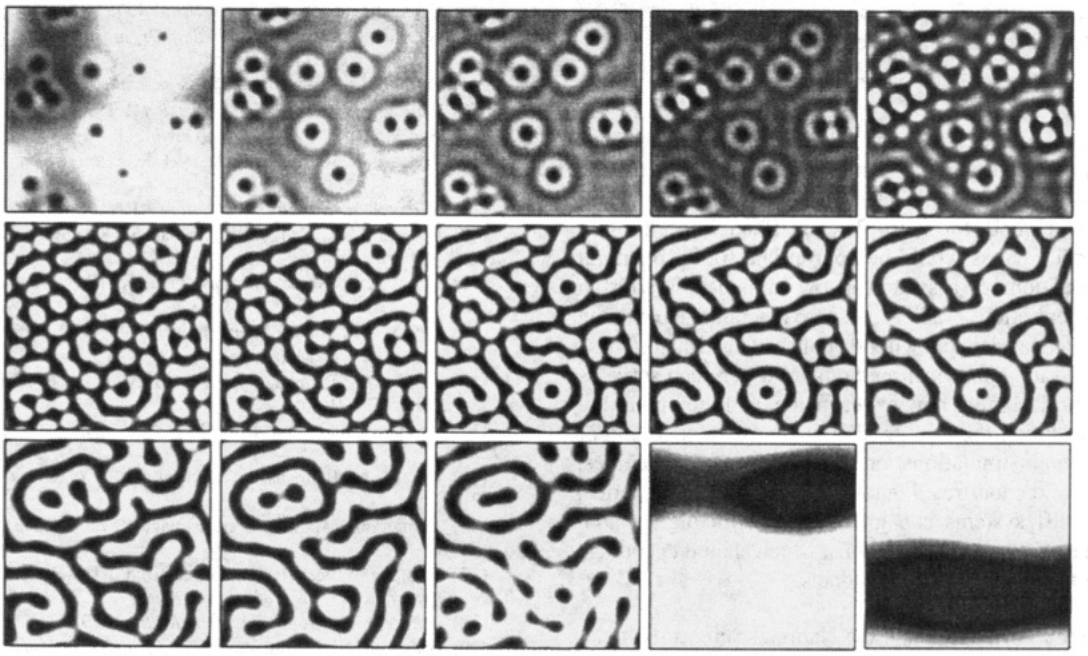

Figure 4. Simulated time development of $[SI_3^-]$ in two spatial dimensions (images at 50 s intervals, 2 mm in length; $[ClO_2]_0 = 6 \times 10^{-3}$ M, $[I_2]_0 = 8.2 \times 10^{-3}$ M, $[H^+] = 10^{-2}$ M, $[MA]_0 = 3.5 \times 10^{-3}$ M). For better contrast, $[SI_3^-]$ is rescaled from 0 to 255 gray levels between its minimum and maximum at each time point.

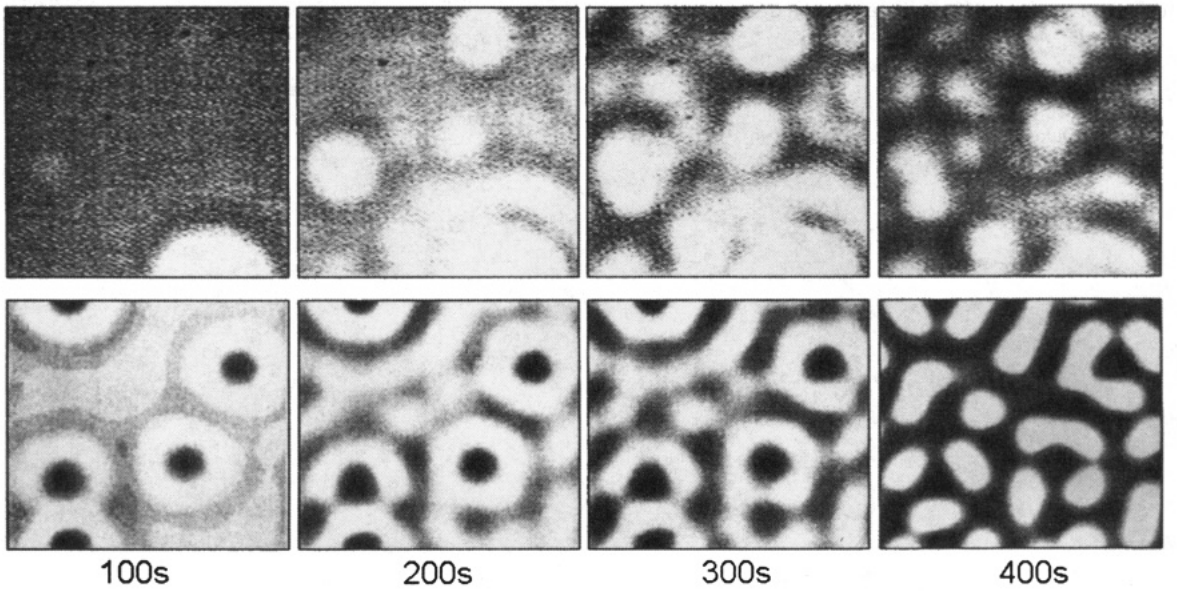

Figure 5. Comparison of experimental (first line) and simulated (second line) time development ($[ClO_2]_0 = 6 \times 10^{-3}$ M, $[I_2]_0 = 8.2 \times 10^{-3}$ M, $[H^+] = 10^{-2}$ M, $[MA]_0 = 4 \times 10^{-3}$ M; length in both is 2 mm).

Figure 3 shows the calculated dependence of the time development on the malonic acid concentration in one spatial dimension. The interpretation of the gray scale is as before. The structures are stable longer at lower malonic acid concentrations; at higher [MA] wave formation and bulk oscillation dominate. The waves do not appear clearly in these simulations, but the presence of homogeneous oscillations suggests that waves are likely to arise in one- or two-dimensional systems of size larger than the wavelength of traveling waves. The wavelength of the Turing structures is 0.15−0.3 mm and increases with the malonic acid concentration, in excellent agreement with the experiments. The other simulated concentration dependences and the time development also agree well with the experimental observations.

Simulations in two spatial dimensions reveal the type of Turing patterns (stripes or hexagons) and how they transform into each other and into waves. In these simulations the two spatial dimensions covered a 2 mm × 2 mm space with 160 × 160 grid points, which gives 80 grid points/mm resolution. The VODPK method, as before, was used to integrate the partial differential equation system, requiring several hours on the workstation for each simulation. The initial concentration of ClO_2 was perturbed by 5% in five randomly chosen cells. Figure 4 shows the concentration pattern of SI_3^- at 50 s intervals for a typical set of initial conditions. At low [MA] (as in Figure 3), the structures persist for quite a long time. At the end of the reaction the structures either fade away ($[MA]_0 \approx 2.0 \times 10^{-3}$M) or they turn into traveling waves ($[MA]_0 \approx 3.5 \times 10^{-3}$M) whose wave speed decreases in time. At higher [MA] the structures live for much shorter times, and waves arise. In Figure 5 we compare the time development of an experimental

and a model system. Despite the poorer resolution of the experimental patterns, the agreement is striking.

Discussion

As noted above, because of the relatively small size of our simulated system, all our calculations were performed with periodic boundary conditions. It is straightforward, however, to adapt this method for zero flux or fixed concentration boundary conditions, as would be appropriate for an open gel reactor. Simulations of a system in two dimensions with an imposed concentration gradient of the reactants have been carried out in this fashion and will be published elsewhere. These simulations and the numerical methods used here can serve as useful tools for designing new experiments, and they point the way toward adapting these methods for more extended and/or three-dimensional simulations on more powerful machines. Finally, we have demonstrated that well-characterized numerical methods for stiff systems can give results with high spatial resolution on inexpensive workstations, which should encourage exploration of realistic chemical models.

Acknowledgment. We thank the National Science Foundation (Grant CHE-9023294) for support of this research. Additional support for this work was provided by a U.S.–Hungarian cooperative grant from the NSF (INT-9322738) and the Hungarian Academy of Sciences and by a grant from the Petroleum Research Fund. We also acknowledge the support of the W. M. Keck Foundation.

References and Notes

(1) Castets, V.; Dulos, E.; Boissonade, J.; DeKepper, P. *Phys. Rev. Lett.* **1990**, *64*, 2953.
(2) Schnackenberg, J. *J. Theor. Biol.* **1979**, *81*, 389.
(3) Nicolis, G.; Prigogine, I. *Self-Organization in Nonequilibrium Systems*; Wiley: New York, 1977.
(4) Dufiet, V.; Boissonade, J. *J. Chem. Phys.* **1992**, *96*, 664.
(5) Dufiet, V.; Boissonade, J. *Physica A* **1992**, *188*, 158.
(6) Borckmans, P.; DeWit, A.; Dewel, G. *Physica A* **1992**, *188*, 137.
(7) Lengyel, I.; Rábai, G.; Epstein, I. R. *J. Am. Chem. Soc.* **1990**, *112*, 9104.
(8) Lengyel, I.; Epstein, I. R. *Science* **1991**, *251*, 650.
(9) Epstein, I. R.; Lengyel, I.; Kádár, S.; Kagan, M.; Yokoyama, M. *Physica A* **1992**, *188*, 26.
(10) Lengyel, I.; Kádár, S.; Epstein, I. R. *Phys. Rev. Lett.* **1993**, *69*, 2729.
(11) Lengyel, I.; Kádár, S.; Epstein, I. R. *Science* **1993**, *259*, 493.
(12) Rovinsky, A.; Menzinger, M. *Phys. Rev. A* **1992**, *46*, 6315.
(13) Jensen, O.; Pannbacker, V. O.; Dewel, G.; Borckmans, P. *Phys. Lett. A* **1993**, *179*, 91.
(14) Lengyel, I.; Epstein, I. R. *Proc. Natl. Acad. Sci. U.S.A.* **1992**, *89*, 3977.
(15) Cesaro, A.; Benegas, J. C.; Ripoll, D. R. *J. Phys. Chem.* **1986**, *90*, 2787.
(16) Yamamoto, M.; Sano, T.; Yasunaga, T. *Bull. Chem. Soc. Jpn.* **1982**, *55*, 1886.
(17) Yamamoto, M.; Harada, S.; Sano, T.; Tatsumoto, N.; Yasunaga, T. *Biopolymers* **1984**, *23*, 2083.
(18) Kaps, P.; Rentrop, P. *Numer. Math.* **1979**, *33*, 55.
(19) Brown, P. N.; Hindmarsh, A. C. *SIAM J. Sci. Statist. Comput.* **1985**, *6*, 297.
(20) Brown, P. N.; Hindmarsh, A. C. *SIAM J. Numer. Anal.* **1986**, *23*, 610.
(21) Byrne, G. D.; Hindmarsh, A. C. *J. Comput. Phys.* **1987**, *70*, 1.
(22) Brown, P. N.; Hindmarsh, A. C. *Appl. Math. Comput.* **1989**, *31*, 40.
(23) Brown, P. N.; Byrne, G. D.; Hindmarsh, A. C. *SIAM J. Sci. Statist. Comput.* **1989**, *10*, 1038.
(24) Kern, D. M.; Kim, C.-H. *J. Am. Chem. Soc.* **1965**, *87*, 5309.
(25) Ruff, I.; Friedrich, V. J.; Csillag, K. *J. Phys. Chem.* **1972**, *76*, 162.

JP9419712